The Mantis Head Camera

(Why the praying mantis is so good at catching its prey)

Igor Katsman, Ehud Rivlin
[igork, ehudr]@cs.technion.ac.il
Department of Computer Science, Technion – IIT 32000, Haifa, Israel.

Abstract

Inspired by the abilities of the praying mantis to judge distance to its prey before the strike by use of motion-based visually mediated odometry, we create miniature model for depth estimation that are similar to the head movements of the Praying Mantis.

We develop mathematical models of the praying mantis behavior and describe our implementations and experimental environment. We investigate structure from motion problem when images are taken from a camera whose focal point is translating according to the biological model. This motion is reminiscent of a praying mantis peering its head left and right, apparently to obtain depth perception, hence the moniker "mantis head camera."

We present the performance of the mantis head camera model and provide experimental results and error analysis of the algorithm. The precision of our mathematical model and its implementation is consistent with the experimental facts obtained from various biological experiments.

I. Introduction

The study of vision guided abilities in insects has become significant not only for entomologists, but also for scientists working in robotics and computer vision who are using unique functional principles learned from the study of insects to develop mathematical models and then, to build an intelligent robot, utilizing these principles for better performance in certain tasks.

The praying mantis provides excellent opportunities for the study of depth estimation by means of self-generated retinal image motion and motion parallax. The biological experimental facts could then form the basis for a biologically relevant mathematical model that would take the experimental findings into account, which could be of assistance for research in computer and robot vision. Thus the eye of a mobile robot could peer from side to side like a praying mantis, to estimate depth for the purpose of avoiding objects and other purposes.

In this paper we focus on robot vision for depth estimation purpose. With the continuously growing development of autonomous robots many groups of researchers (both engineers and biologists) conducted studies in different directions of biologically inspired robotics vision. Generally, work in this domain could be classified to top-down (e.g. [13]) and bottom-up (e.g. [21]). In the top-down approach a certain task, such as path planning [7], visual mediated odometry [3], etc. looks for inspiration in biological model. Where in the bottom-up approach, a certain biological behavior, such as visual mediated navigation [15, 21], visual mediated flight control [23, 15], etc. are directly modeled with real robots. Our work belongs to the bottom-up approach.

The work presented here can be thought of as part of an attempt to model the visual behavior of the Praying Mantis. Number of studies of formal behavioral models (such as schema-theoretic model) of the praying mantis were presented [4, 5]. In these studies, several visually mediated activities or behaviors of the praying mantis such as prey acquisition, predator avoidance, mating and Chantlitaxia were formulated in details. Each of the above behaviors could be implemented by set of visual-based functions, one of which is investigated here. Several experimental biologic studies researching the visual abilities and behaviors of the Praying Mantis were presented in [17, 24]. The precision of our mathematical model and its implementation is consistent with the experimental facts obtained from various biological experiments.

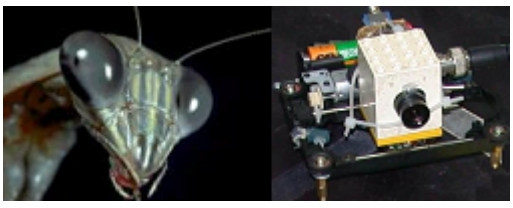

Figure1: Mantis Head versus Mantis Head Camera.

In this paper we develop a mathematical model of the biologically motivated visual-motor system for depth estimation; we describe an implementation of the system and experimental environment; we present and discuss the performance of the system and provide experimental results and error analysis of the algorithm; we present the conclusions and propose potential usage of the system in mobile robot environment.

II. THE MODEL

Figure 2.1 illustrates the process. The camera moves left and right (pure translation) along the X-axis according to the function $c = c(t)$, where we set $c = c(0)$. Typically this motion is with constant speed (and changing direction at the edges of the platform) such as $c(\tau) = s * V_0 * \tau$, where s is 1 or -1 depending on the peering direction.

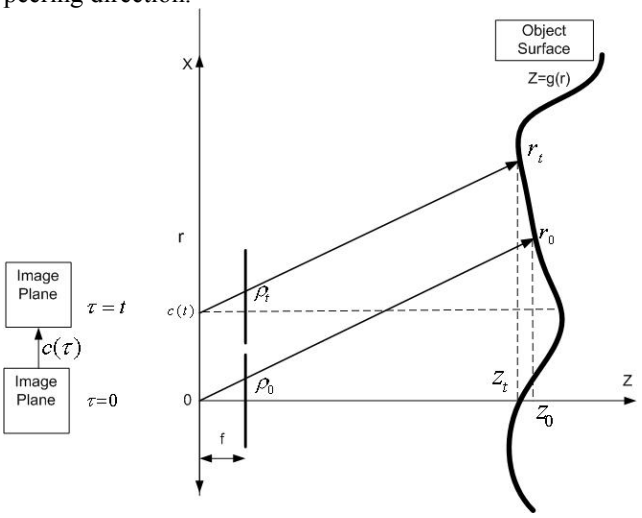

Figure 2.1: Mantis head camera model. The surface, which cross-section, is given by $z = g(r)$, is viewed by a camera with focal point moving along the X-axis. ρ denotes the displacement along the X-axis from the CCD center on the image plane at which a feature is projected, and $r_0(\rho)$ and $r_t(\rho)$ are the displacements where points observed at the displacement ρ on the image plane are located on the surface of the object.

We start from the following relationship, where *f* is the focal length of the camera:

$$\frac{\rho}{f} = \frac{r}{z}.$$

When the camera is in its initial position ($\tau = 0$):

$$\frac{\rho}{f} = \frac{r_0}{z_0}.$$

For $\tau = t$, when the camera is displaced along the X-axis according to the function $c(t)$ we have:

$$\rho = f\frac{r_t - c(t)}{z_t} = f\frac{r_t - c(t)}{g(r_t)},$$

in the same coordinate system. Whence,

$$\frac{1}{f}\rho g(r_t) = r_t - c(t),$$

or

$$r_t = \frac{1}{f}\rho g(r_t) + c(t). \qquad (2.1)$$

In the most general case we define the inverse function as:

$$r_t = h_c(\rho). \qquad (2.2)$$

The image might be regarded as a function of *r* which itself is a function of time and ρ, say $I = F(r_t) = F(h_c(\rho)) = F(h_c(t)(\rho))$.

Useful information can be obtained by observing the ratio of the derivatives of I with respect to ρ and t.

$$\frac{\frac{\partial I}{\partial \rho}}{\frac{\partial I}{\partial t}} = \frac{\frac{\partial F(r_t)}{\partial \rho}}{\frac{\partial F(r_t)}{\partial t}} = \frac{F'(h_c(\rho))\frac{\partial h_c}{\partial \rho}}{F'(h_c(\rho))\frac{\partial h_c}{\partial t}} = \frac{\frac{\partial h_c}{\partial \rho}}{\frac{\partial h_c}{\partial t}}. \qquad (2.3)$$

To evaluate (2.3) we combine (2.1) and (2.2) to obtain

$$h_c(\rho) = r_t = \frac{1}{f}\rho g(r_t) + c(t) = \frac{1}{f}\rho g(h_c(\rho)) + c(t)$$

Differentiation with respect to ρ and t yields

$$\frac{\partial h_c(\rho)}{\partial \rho} = \frac{1}{f}(\rho g'(h_c(\rho))\frac{\partial h_c(\rho)}{\partial \rho} + g(h_c(\rho))),$$

and

$$\frac{\partial h_c(\rho)}{\partial \rho} = \frac{\frac{1}{f}g(r_t)}{1 - \frac{1}{f}\rho g'(r_t)}; \qquad (2.4)$$

$$\frac{\partial h_c(\rho)}{\partial t} = \frac{1}{f}\rho g'(h_c(\rho))\frac{\partial h_c(\rho)}{\partial t} + \frac{dc}{dt}, \text{ and}$$

$$\frac{\partial h_c(\rho)}{\partial t} = \frac{\frac{dc}{dt}}{1 - \frac{1}{f}\rho g'(r_t)}. \qquad (2.5)$$

From (2.3), (2.4), and (2.5) it follows that:

$$\frac{\frac{\partial I}{\partial \rho}}{\frac{\partial I}{\partial t}} = \frac{\frac{\partial h_c}{\partial \rho}}{\frac{\partial h_c}{\partial t}} = \frac{\frac{\frac{1}{f}g(r_t)}{1 - \frac{1}{f}\rho g'(r_t)}}{\frac{\frac{dc}{dt}}{1 - \frac{1}{f}\rho g'(r_t)}} = \frac{\frac{1}{f}g(r_t)}{\frac{dc}{dt}}, \qquad (2.6)$$

$$g(r_t) = z_t = f\frac{dc}{dt}\frac{\frac{\partial I}{\partial \rho}}{\frac{\partial I}{\partial t}}. \qquad (2.7)$$

In this expression $c = c(t)$ and $\frac{dc}{dt}$ are given, while $\frac{\partial I}{\partial \rho}$ and $\frac{\partial I}{\partial t}$ are determined by observation.

III. EXPERIMENTAL ENVIRONMENT

A miniature video camera was mounted on a specially designed micro-translation platform, which provides precise periodic side-to-side peering movements of the camera with constant speed. When an electromotor of the platform is activated, the camera translates in the direction that is parallel to the image plane. This behavior simulates the peering behavior of the praying mantis.

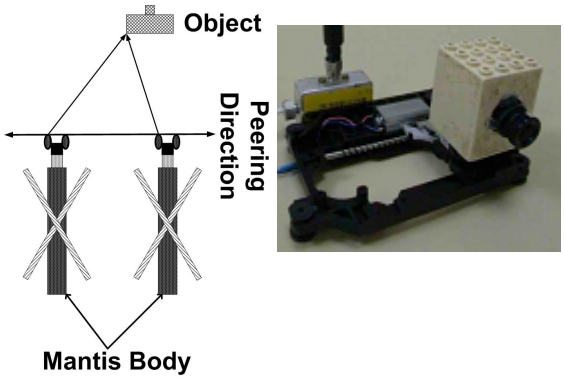

Figure 3.1: Scheme of Peering Behavior of Praying Mantis and the implementation of the Miniature Mantis Head Camera Platform, which utilizes peering behavior for distance estimation

The video output signal of the camera is connected to the miniature wireless video RF transmitter, which broadcasts video signal remotely, thus enabling autonomic usage of the device on mobile robot. Both camera and transmitter are operated from single 9v battery. The total size of the platform with camera and transmitter is [10cmx5cmx2cm]. The video signal is then received by an RF video receiver that is connected to the PCI frame grabber located inside a Dual Pentium III workstation, which performs the image processing of all the incoming frames. In addition, based on the incoming image analysis, the workstation could send action commands back to the remote robot, supporting the peering platform.

Varying the target distance and peering velocity parameters, performance of the system was measured. Targets were placed at various distances in front of the camera: 5, 6, 7, 8, 9, and 10 cm. Peering velocities of 1.5cm/sec and 2cm/sec were used.

[For *Mantis Religiosa* individuals 50 to 70 mm in size, peering amplitudes are approximately 2 to 10 mm and peering velocities approximately 6 to 18 mm s^{-1}.]

IV. EXPERIMENTAL RESULTS

Optic flow is a visual displacement flow field that can be used to explain changes in an image sequence. The underlying assumption used to obtain an equation is that the gray level is constant along the visual trajectories. In other words, the partial derivative of the gray level $I_t(x,y)$ along the optic flow

$V = (v_1, v_2) = (\frac{dx}{dt}, \frac{dy}{dt})$ is zero:

$$\frac{\partial I_t}{\partial x}\frac{dx}{dt} + \frac{\partial I_t}{\partial y}\frac{dy}{dt} + \frac{\partial I_t}{\partial t} = 0 . \qquad (2.8)$$

This equation alone is not sufficient to determine a unique vector field, since at any location we have only a single scalar constraint with which to find a two-dimensional vector (v_1, v_2), which constitutes an ill-posed problem.

Since in our case the camera moves along the X-axis (with constant speed $\frac{dc}{dt}$), the component of the velocity $\frac{dy}{dt}$ along the Y-axis is zero, so we can reduce equation (2.8) to the following: $\frac{\partial I_t}{\partial x}\frac{dx}{dt} + \frac{\partial I_t}{\partial t} = 0$, i.e.

$$\frac{dx}{dt} = -\frac{\frac{\partial I_t}{\partial t}}{\frac{\partial I_t}{\partial x}} . \qquad (2.9)$$

Using (2.9) one can rewrite equation (2.7) as (denoting $\rho = x$): $g(r) = z = -f\frac{\frac{dc}{dt}}{\frac{dx}{dt}} = -f\frac{sV_0}{v_1}$. (2.10)

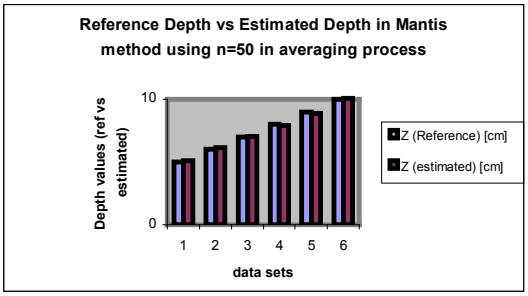

Figure 4.1: Reference distance versus averaged estimated distance.

According to (2.10), when the observer moves with speed V_0, the retinal images of objects close to the eye (smaller z) are displaced more quickly (bigger v_1) than those of more distant objects (bigger z).

In other words, in the case of a visual field comprised of stationary objects, retinal image motion and motion parallax initiated by the observer can be used to determine the absolute and relative distance of objects.

In the case of the praying mantis, translatory side-to-side movements of the head in a horizontal plane are performed to determine the jump distance to stationary objects. The speed of the retinal image motion is the relevant parameter for determining the distance to the

object; thus, by computing the above optic flow one can estimate the distance to the objects.

There are two main approaches to computing optic flow: Token matching or correlation (extracting features from each frame and matching them from frame to frame) and Gradient techniques (relating optic flow to spatial and temporal image derivatives). Gradient-based methods only work when the motion is "small" and the derivative can be reliably computed. Note that for "large" motion one can employ multi-resolution methods. Tracking algorithms can compute motion when the motion is "large" by using correlation based methods or feature tracking. In our model we used the token matching approach.

In our experiments the target object was placed at various known distances in front of a constantly peering camera. The distance to the object was estimated by computing v_1 in equation (2.10) via the token matching (fast feature tracking) technique. The experimentally estimated distances were compared to their true values and the accuracy of the estimations was calculated.

For each peer of the camera the object was sampled n=50 times with constant frame rate of 30 Hz, and the average v_1 was computed as $v_1 = \frac{1}{n}\sum_{i=1}^{i=n} v_{1i}$, which greatly improves the accuracy of the estimation algorithm.

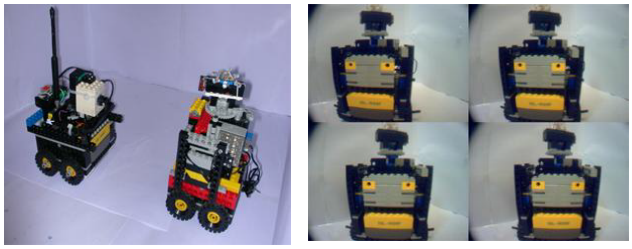

Figure 2.4: Tiny Lego Robot utilizes Miniature Mantis Head Camera. Sequence order: top left, top right, bottom left, bottom right.

Figure 2.5: Two subsets (of 4 samples each) captured during left to right peer of the Mantis Head Camera Platform. (Nature scenarios). Sequence order: top left, top right, bottom left, bottom right

.

V. ERROR ANALYSIS

In what follows we discuss the sources of inaccuracy of the described algorithm. Then a scheme for accuracy evaluation of the estimated depth will be proposed.

The algorithm presented here requires flow calculation; therefore the approximation accuracy of v_1 in expression (2.10) has a critical role for the depth estimation accuracy. The approximate precision of v_1 is mainly determined by noise and quantization. The influence of these two factors is investigated below.

The deviation in the camera motion speed is another factor, which also has a significant impact on the algorithm accuracy. The algorithm assumes a precise mechanical setup, i.e. constant camera motion speed. However, this assumption was difficult to satisfy absolutely. The influence of this factor on the algorithm accuracy is also investigated.

Let $\hat{v}$ and $\hat{u}$ be the approximated retinal images and observer velocities, respectively. Then the absolute error in the depth estimation ΔZ can be calculated using the following equation, obtained from (2.10). (For brevity, we introduce $k = -fs$ in all equations below):

$$g(r) = Z = k\frac{u}{v}, \qquad (2.11)$$

where $u = \frac{dc}{dt}$, $v = \frac{dx}{dt}$.

$$\Delta Z = \hat{Z} - Z = k\left(\frac{\hat{u}}{\hat{v}} - \frac{u}{v}\right). \qquad (2.12)$$

Let δ_u, δ_v be the relative errors in the approximation:

$$\begin{pmatrix} \delta_u \\ \delta_v \end{pmatrix} \triangleq \begin{pmatrix} \frac{\hat{u}-u}{u} \\ \frac{\hat{v}-v}{v} \end{pmatrix} \qquad (2.13)$$

Then,

$$\hat{u} = u\delta_u + u = (1+\delta_u)u$$

$$\hat{v} = v\delta_v + v = (1+\delta_v)v.$$

Using the above notation and (2.12) we obtain:

$$\Delta Z = \hat{Z} - Z = k\left(\frac{(1+\delta_u)u}{(1+\delta_v)v} - \frac{u}{v}\right),$$

which can be simplified to:

$$\Delta Z = k\frac{u}{v}\left(\frac{(1+\delta_u)}{(1+\delta_v)} - 1\right) = k\frac{u}{v}\left(\frac{(\delta_u - \delta_v)}{(1+\delta_v)}\right) \qquad (2.14)$$

Now, letting the upper bound of $|\delta_v|$ be M, and denoting B to be the following constant

$$B = \frac{1}{1-M}, \qquad (2.15)$$

(2.14) implies:

$$\Delta Z \approx Z(\delta_u - \delta_v) \text{ and}$$
$$|\Delta Z| \le |Z|(|\delta_u| + |\delta_v|)B \ . \qquad (2.16)$$

To estimate the expected depth calculation error, we insert the standard deviation σ_u and σ_v into the error expressions δ_u and δ_v:

$$|\delta_u| = \frac{\sigma_u}{|u|} \text{ and } |\delta_v| = \frac{\sigma_v}{|v|} \ .$$

The relative error δ_Z of the estimated depth can be evaluated using the relations above and (2.16):

$$\delta_Z = \frac{\hat{Z} - Z}{Z} = \frac{\Delta Z}{Z} \ ,$$
$$|\delta_Z| \le \left(\frac{\sigma_u}{|u|} + \frac{\sigma_v}{|v|}\right)B \approx \frac{\sigma_u}{|u|} + \frac{\sigma_v}{|v|} \ . \qquad (2.17)$$

(2.17) gives a rough evaluation of the accuracy of the estimated depth in (2.10). Sampling *n* times, during each peer of the camera, and computing the average v_1 according to $v_1 = \frac{1}{n-2k}\sum_{i=k+1}^{i=n-k} \overleftrightarrow{v}_{1i}$, where $\overleftrightarrow{v}_{1n}$ is sorted v_{1n}, greatly improves the accuracy of the estimated depth.

In this part we will investigate the expected accuracy of the proposed depth estimation method. This accuracy evaluation is based on the algorithm implementation scheme described before.

At first, we will concentrate on the imaging factor $\hat{v}$ of the algorithm's expected inaccuracy. The inaccuracy of this term is caused by several factors: The image function $I(\rho,t)$ is given on a discrete grid and not on a continuous one. The values of the function $I(\rho,t)$ are quantized. The values of the function $I(\rho,t)$ are noisy.

We use synthetic image sequences for the estimation of the quantization and noise influence. The generated images were degraded with a Gaussian additive noise with mean $\mu = 0$ and variance σ^2, with the noise values at two different pixels being independent. The $\hat{v}$ approximations of the degraded data were calculated and compared to the ideal $\hat{v}$ values (without noise and quantization). The mean square value of the error was calculated for the different values of noise variance σ^2 and neighborhood size. The received values of the approximation errors of $\hat{v}$ are shown in Figure 4.6. This table demonstrates the approximation accuracy as a function of noise variance σ^2 and neighborhood size used for $\hat{v}$ approximations. The error values shown in the columns corresponding to $\sigma^2 = 0$ are approximation errors caused by quantization only.

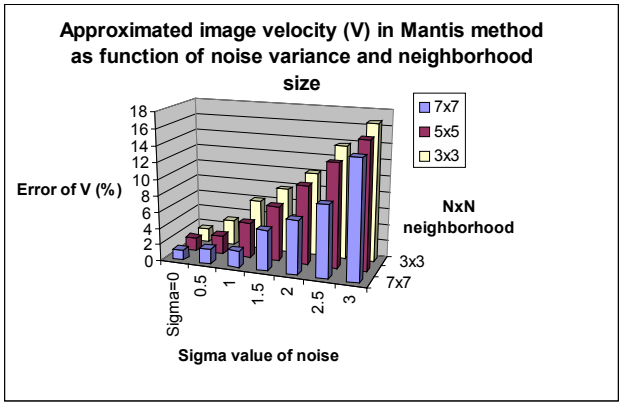

Figure 4.6. The simulation-based errors of the depth estimation as a function of the noise variance σ^2 and neighborhood size used for the approximation of $\hat{v}$. The first column $\sigma = 0$ shows the error values caused by quantization only.

From Figure 4.6-[graph series] it follows that for a camera characterized by a 1% noise (~2.0 grey level per pixel), which is typical for real cameras, the accuracy of the depth estimation is about 2%.

The inaccuracy in the observer velocities $\hat{u}$ is due to the speed of the camera not being constant.

This value is determined by counting the number of frames between the border frames (frames with no motion detected). There could be an error of 2 frames from a total of 66 frames in this procedure. Using this calibration procedure a number of times and applying simple averaging on the noisy results, the estimated error of the observer is about 1%.

From the above calculations it follows that one can expect a depth estimation error of about 3% from the actual camera setup.

This expectation is consistent with the errors in the depth estimation values obtained from the algorithm's execution.

VI. CONCLUSIONS

In this study a biologically motivated mathematical model of depth estimation and its implementation were presented. We showed how one can recover depth using peering behavior that is commonly used by the praying mantis. The model is consistent with recent behavioral and anatomical evidence collected from various biologic experiments with the praying mantis [17, 24]

The presented system can estimate a depth to a set of objects, similarly to the ability of praying mantis, which can be used by mobile agent for learning the surrounding space, collision avoidance and navigation. The real-time performance of the model adds to its attractiveness for usage with mobile agents.

The miniature and extremely light mechanical, optical and electronic implementation of the model was presented. This property makes it possible to install it on

top of small mobile robot or smaller vehicle and use it to obtain depth information of points of interest in the surrounding space.

The single percent precision depth estimation, achieved by the model and its implementation, are consistent with both the results of error analysis and those demonstrated by live praying mantis during its prey catching process.

As items for future work, we plan to investigate other visual routines of the praying mantis. Particularly, we plan to use our mantis head platform mounted on miniature mobile robot in order to implement some of the visual behaviors of the praying mantis, as presented by Arkin et al [4]. We also plan to implement some of the real-time indoor navigation algorithms [20, 16] using Lego mobile robots with the mantis head platform. Using precise distance estimation by the platform, Lego robots will be available to perform an accurate docking and other precision requiring tasks, which are difficult to achieve with standard Lego environment. As another direction for future work, we plan to study the principles of different types of self motion for precise depth estimation used by other animals, measure their sensitivity, evaluate precision and compare to that used by the praying mantis.

In this study, we have developed a mathematical model of the biologically motivated visual-motor system for distance estimation, then described an implementation of the system and experimental environment, presented and discussed the performance of the system and experimental results, provided an error analysis of the algorithm and its high precision, which is consistent with that of the praying mantis, and presented directions for the future work.

VII. REFERENCES

[1] Ali, K.S. and Arkin, R.C., 1998, "Implementing schema-theoretic models of animal behavior in robotic systems," *5th International Workshop on Advanced Motion Control – AMC '98*, Coimbra, Portugal, pp. 246 –254.

[2] Aloimonos, Y., 1993, "Active vision revisited". "*Active perception*" Book, Lawrence Erlbaum associates, publishers. Hillsdale, New Jersey.

[3] Argyros, A. A., Bekris, C., and Orphanoudakis, S.O., 2001, "Robot homing based on panoramic vision", *TR287 ICS-FORTH*.

[4] Arkin, R.C., Ali, K.S., Weitzenfeld A., Cervantes-Perez F., 2000, "Behavioral Models of the Praying Mantis as a Basis for Robotic Behavior." *Journal of Robotics and Autonomous Systems*, 32 (1), pp. 39-60.

[5] Arkin, R.C., 1997, "*Ecological Robotics*: A Schema-theoretic Approach". Sensing, Modelling and Planning, eds. R.C. Bolles, H. Bunke, and H. Noltemeier, World Scientific, pp. 377-393.

[6] Bruckstein, A.M., Holt, R.J., Huang, T.S., and Netravali, A.N., 2000, "New Devices for 3D Pose Estimation: Mantis Eyes, Agam Paintings, Sundials, and Other Space Fiducials". *International Journal of Computer Vision* 39(2): 131-139.

[7] Chameron, S., Beugnon, G., Schatz, B., and Collett, T.S., 1999, "The use of path integration to guide route learning in ants". *Nature*, Vol. 399, N° 6738.

[8] Chaumette, F., Boukir, S., Bouthemi, P., and Juvin, D., 1996, "Structure from controlled motion", *PAMI(18),* No. 5, pp. 492-504.

[9] Cheong, L.F., and Xiang, T., 2001, "Characterizing depth distortion under different generic motions", *International Journal of Computer Vision*, 44(3), pp. 199-217.

[10] Dalmia, L.K. and Trivedi, M., 1996, "High speed extraction of 3D structure of selectable quality using a translating camera". *Computer Vision and Image Understanding*, Vol. 64, pp.97-110.

[11] Davies, M.N.O. and Green, P.R., 1991. "The adaptability of visuomotor control in the pigeon during flight." *Zool. Jahrb., Physiol.*, 95: 331-338.

[12] Dellaert, F., Seitz, S.M., Thorpe, C.E., Thrun, S., 1999, "Structure from Motion without Correspondence", *IEEE, CVPR00* pp. 557-564.

[13] Franceschini, N., Pichon, J. M., and Blanes, C., 1992, "From insect vision to robot vision," *Phil. Trans. R. Soc. Lond. B,* 337, pp. 283-294.

[14] Frost, B.J., 1978. "The optokinetic basis of head-bobbing in the pigeon." *J. Exp. Biol.*, 74: 187-195.

[15] Iida, F., 2001, "Goal-Directed Navigation of an Autonomous Flying Robot Using Biologically Inspired Cheap Vision," *Proceedings of the 32nd ISR (International Symposium on Robotics)*, 19-21.

[16] Kamon, I., Rimon, E., and Rivlin, E., 1998, "Tangent Bug: A Range-Sensor-Based Navigation Algorithm." *International Journal of Robotic Research*, 17(9), pp. 934-953.

[17] Kral, K., 1998, "Side-to-side head movements to obtain motion depth cues: A short review of research on the praying mantis," *Behavioural Processes* 43 71–77.

[18] Lambrinos, D., Möller, R., Labhart, T., Pfeifer, R., and Wehner, R., 2000, "A mobile robot employing insect strategies for navigation." *Robotics and Autonomous Systems, special issue on Biomimetic Robots*, 30:39-64.

[19] Lenz R.K. and Tsai R.Y., 1987, "Techniques of calibration of the scale factor and image center for high accuracy 3d machine vision metrology." *Proceedings of IEEE International Conference on Robotics and Automation.*

[20] Lumelsky, V. and Skewis, T., 1990, "Incorporating Range Sensing in the Robot Navigation Function", *IEEE Transactions on Systems, Man and Cybernetics,* Vol. 20, No. 5., pp. 1058–69.

[21] Moller, R., Lambrinos, D., Roggendorf, T., Pfeifer, R., and Wehner, R., 2000, "Insect strategies of visual homing in mobile robots." In: *T. Consi, B. Webb: Biorobotics*, AAAI Press.

[22] Sandini, G., and Tistarelli, M., 1990, "Active Tracking Strategy for Monocular Depth Inference over Multiple Frames", *IEEE, PAMI,* pp. 13-27.

[23] Srinivasan, M. V., Lehrer, M., Kirchner, W., Zhang, S. W., and Horridge, G. A., 1988, "How Honeybees use Motion Cues to Estimate the Range and Distance Objects," Proc. *IEEE SMC* pp. 579-582, (in English).

[24] Yamawaki, Y., 2000, "Effect of luminance, size and angular velocity on the recognition of non-locomotive prey models by the praying mantis," Japan Ethological Society and Springer Verlag.

[25] Zheng, W., Kanatsugu, Y., Shishikui, Y., Tanaka, Y., 2000, "Robust Depth-map Estimation from Image Sequences with Precise Camera Operation Parameters", *ICIP00*.